Analysis of Plasma Detachment through Magnetic Nozzle via Canonical Field Theory

Yu Takagaki

A thesis
submitted in partial fulfillment of the
requirements for the degree of

Master of Science in Aeronautics and Astronautics

University of Washington

2017

Committee

Setthivoine You

Uri Shumlak

Program Authorized to Offer Degree:

Aeronautics and Astronautics

University of Washington

Abstract

Analysis of Plasma Detachment through Magnetic Nozzle via Canonical Field Theory

Yu Takagaki

Chair of the Supervisory Committee:
Assistant Professor Setthivoine You
Aeronautics and Astronautics

In this paper, I have investigated the mechanism of plasma detachment through magnetic nozzle via canonical field theory, especially by considering canonical vorticity flux Ψ_σ contour and dissipative force $\vec{R}_\sigma$. As one of the most recent experimental proofs of plasma detachment, Olsen et al[5]., observed and investigated three key indications of plasma detachment. However, after solving for numerical fits with their experimental data, I found that constant ion flux lines did not actually separate from constant magnetic flux lines. Thus, their first key indication becomes incorrect now. Whereas, my analytical results are consistent with the other two key indications. At the beginning, plasma detached from canonical vorticity flux contours due to non-zero dissipative force and attached on magnetic flux lines instead. However, $\vec{R}_\sigma \simeq 0$ force makes plasma re-attach on canonical vorticity flux contours around the plume edge region. As the most significant and notable result through my analysis, I confirmed the existence of returning plasma flow around the plume edge region.

TABLE OF CONTENTS

Page

List of Tables iii

List of Figures iv

Chapter 1: Introduction 1

Chapter 2: Overview of Plasma Detachment through Magnetic Nozzle 3
2.1 What is Plasma Detachment 3
2.2 Historical Research Progress on Magnetic Nozzle and Plasma Detachment . . 4

Chapter 3: Plasma Detachment observed in VASIMR Research 8
3.1 Experimental Setup 8
3.2 Experimental Results and Discussion 10
3.3 Summary of VASIMR VX-200 Research 18

Chapter 4: Canonical Field Theory 19
4.1 Governing Equations 20
4.2 Frozen-in Theorem for Canonical Field Theory 21

Chapter 5: Analysis of Plasma Detachment via Canonical Field Theory 24
5.1 Constant Ion Flux Contour 24
5.2 Canonical Vorticity Flux Contour 29
5.3 Summary of Analysis 33

Chapter 6: Summary 35

Appendix A: Frozen-in Theorem 37

Appendix B: Constant $\Gamma_{iz}\left(r_{edge}\right)$ case 38

Bibliography 40

LIST OF TABLES

Table Number Page

4.1 Comparison of governing equations between MHD Theory and Canonical Field Theory 22

4.2 One-to-one relationships between MHD Theory and Canonical Field Theory 23

LIST OF FIGURES

Figure Number — Page

3.1 Conceptual schematic of VASIMR VX-200 engine[5] 9
3.2 Image of plasma diagnostics[5] 10
3.3 "Illustrating the method of spatially tracking lines of constant integrated ion flux and magnetic flux. Convergent detachment is shown (x-section insets) and appears as ion flux (pink) expanding slower than magnetic flux (blue)"[5]. 11
3.4 "Standard shot configuration including uncertainty bounds (dashed lines). Data analysis windows for the low- and high-power configurations were taken from 0.4− 0.5 and 0.65− 0.75 s, respectively. Top: average RF forward power profile. Middle: steady 3600-sccm (~ 107 mg/s) argon flow. Bottom: exhaust region chamber pressure measured by separate hot cathode ion gauges."[5] . 13
3.5 Lines of constant f_i (red solid) during the helicon + ICH operation compared with lines of constant enclosed magnetic flux (black dashed)[5] 14
3.6 Possible shapes of plasma plume and r_{edge} 15
3.7 Contour maps of the ion velocity distribution function as a function of v_r and v_z at five radial locations and $z = 3.9\,[m]$. "The local magnetic field vector is overlain in each plot (black arrow)"[5] 16
3.8 "Image summarizing various regions associated with detachment process. The flow lines (blue) are based on the integrated ion flux fraction and extended out along the linear region. Lines showing the transition above unity for kinetic and thermal beta are displayed for reference (red dashed)"[5] 17
5.1 Comparison for the strength of magnetic field on z-axis for vacuum case (black), helicon only case (blue), and helicon + ICH case (red) in experiments and my analytical one (green)[5] 25
5.2 Comparison for experimental magnetic flux lines (black dashed), experimental magnetic flux fraction f_i lines (red) and my analytical magnetic flux (blue dashed)[5] 26
5.3 Axial ion current density contour map 26

5.4 Comparison between experimental ion flux fraction f_i lines (red) and my analytical f_i lines (blue) with experimental magnetic flux ψ lines (black dashed) and analytical magnetic flux ψ lines (light blue dashed)[5] 27
5.5 number density contour map with r_{edge} (yellow dashed). Red point indicates the basepoint of r_{edge} 27
5.6 number density contour map with r_{edge} (yellow dashed). Red point indicates the basepoint of r_{edge} 28
5.7 n_i contour map with constant ion flux $\Gamma_i(r)$ lines (blue solid), constant magnetic flux ψ lines (light blue dashed), and r_{edge} (yellow dashed) 29
5.8 n_i contour map with constant canonical vorticity flux Ψ_i lines (orange), constant ion flux $\Gamma_i(r)$ lines (blue), constant magnetic flux ψ lines (light blue dashed), and r_{edge} (yellow dashed) 31
5.9 Summary of plasma detachment via canonical force field theory 34

B.1 Axial ion current density contour map 38
B.2 Comparison between experimental ion flux fraction f_i lines (red) and my analytical f_i lines (blue) with experimental magnetic flux ψ lines (black dashed) and analytical magnetic flux ψ lines (light blue dashed)[5] 39
B.3 number density contour map with r_{edge} (yellow dashed). Red point indicates the basepoint of r_{edge} 39

ACKNOWLEDGMENTS

First and foremost, I would like to thank my research advisor Professor Setthivoine You at University of Washington for giving me the chance to work for him. While I did not have strong background in plasma physics, he allowed me to participate in one of his research, and I could learn a lot of fundamental and practical stuff through our research and his classes. It has been an honor to make some contributions to him and his research, and it would indeed be a pleasure that his canonical field theory will become widely recognized.

I would also like to thank Eric Sander Lavine for always being supportive and giving me quite helpful advice. Without his guidance, knowledge and inteligence, my analytical research could not have been successfully conducted. As one of his friends, I do hope for his academic success.

I would also like to acknowledge Professor Uri Shumlak at University of Washington for giving me some invaluable advice and comments as the second reader of my thesis. He always kindly and friendly listened to my research progress and guided me to the right direction. It will be a great pleasure that he will welcome me to one of his research projects and I'm looking forward to working with him.

Lastly, I would like to give my profound gratitude to my parents for being extremely supportive and providing unfailing encouragement from Japan throughout my graduate school life.

DEDICATION

to my parents, Yasuo and Machiko

Chapter 1

INTRODUCTION

In the 1920s, the Noble prize laureate Irving Langmuir pioneered the scientific study of plasma. Around the 1940, after Hannes Alfvén developed the MagnetoHydroDynamics (MHD) theory to understand various astrophysical phenomena, plasma came to be treated essentially as a conducting fluid. In the 1950s, plasma physics reached a certain major turning point. The production of power from thermonuclear fusion has been suggested as one of the most promising application of plasma, and plasma physics theory has been widely and successfully developed[8][78].

For other practical purposes, plasma jets started to be widely used in manufacturing (e.g., metallurgical and chemical purposes) and electric propulsion fields. Electric propulsion is one of the most promising devices for a deep space exploring mission and a manned interplanetary mission. To produce high specific impulse and relatively larger thrust with high efficiency, plasma flow is generally guided and controlled by properly shaped electromagnetic fields. In particular, nozzle shaped magnetic field is called a "magnetic nozzle." Like a physical nozzle, a magnetic nozzle produces sub-to-super sonic transition through converging and diverging shape of the nozzle. Also, it can achieve even sub-to-super Alfvénic transition when we have enough energy. Thus, a magnetic nozzle can essentially work as a nozzle with a flexible wall. Whereas interactions between plasma flow and applied or self-generated electromagnetic fields produce additional complexities and difficulties to fully control plasma jets. Therefore, it is quite important to understand physics of plasma jets through a magnetic nozzle.

In this paper, I will utilize canonical field theory to investigate whole physics of plasma jets,

especially plasma detachment instead of using typical two-fluid model or MHD theory. In section 2, I will explain an overview of plasma detachment issues; section 3 presents VASIMR experimental investigations as some of the most recent research on plasma detachment; in section 4, I will introduce key definitions and equations for canonical field theory; section 5 produces analytical results via canonical field theory which are consistent with experimental ones; in section 6, I will give my conclusion and summary of this paper.

Chapter 2

OVERVIEW OF PLASMA DETACHMENT THROUGH MAGNETIC NOZZLE

2.1 What is Plasma Detachment

The simplest method of controlling plasma flow through a magnetic nozzle is using frozen-in theorem. In ideal MHD theory, total magnetic flux ψ through a certain closed contour is constant in the frame moving with plasma. Magnetic flux is defined by

$$\psi \equiv \int \vec{B} \cdot d\vec{S} \tag{2.1}$$

where $\vec{B}$ is magnetic field and $d\vec{S}$ is a vector element of area of closed contour. The change in ψ is

$$\frac{d\psi}{dt} = \frac{\partial \psi}{\partial t} + (\vec{v} \cdot \nabla)\, \psi = \oint (\vec{u} - \vec{v}) \times \vec{B} \cdot d\vec{l} = 0 \tag{2.2}$$

where $\vec{u}$ and $\vec{v}$ are plasma velocity and reference frame velocity, respectively. From Eq. 2.2, I can present the typical statement; magnetic flux is frozen-in plasma.

On the other hand, for some practical purposes, especially for propulsion, we want to make plasma detach from magnetic flux contour. Otherwise we cannot obtain net thrust because plasma will move with a closed magnetic flux contour. This issue is called as "plasma detachment," and is one of the biggest challenges in a propulsion field. In short, plasma detachment cannot be simply explained by using ideal MHD theory.

2.2 Historical Research Progress on Magnetic Nozzle and Plasma Detachment

Until the 1950s, ideas for many different types of electric propulsion had been introduced and developed. At the same time, a concept of magnetic nozzle was proposed for more practical purposes. In the 1960s, as an initial approach to understand notable characteristics of a magnetic nozzle, Chu[12] analyze sub-to-super sonic transition and sub-to-super Alfvénic transition for infinitely conducting plasma via single fluid model. Through his analysis, he confirmed the existences of those transitions through a magnetic nozzle like a physical nozzle for neutral fluids. Also, Andersen et al.[13], built experimental magnetic Laval nozzle and produced supersonic plasma flow. Otis[14] observed Hall potential due to an interaction between supersonic plasma flow and guiding magnetic field.

During the 1970s, Kuriki and Okada[15] measured a potential barrier due to Hall parameter and an additional ion acceleration to an isentropic expanding magnetic nozzle case. Gohda[16] numerically solved MHD equations to investigate the interactions between shock-heated plasma flow and a magnetic nozzle via two-step Lax-Wendroff method. In 1977, F. R. Chang Diaz proposed the VASIMR engine concept. While a strong research progress on a magnetic nozzle could not be seen during the 1980s, a concept of magnetic nozzle became more popular and was widely applied in propulsion and manufacturing fields (e.g., welding, cutting, solid waste processing and plasma deposition).

In response to active research on electric propulsion, magnetic nozzle research also became a major research topic in plasma physics. As the theoretical research, Power[17] designed Microwave Electrothermal Thruster (MET) with a magnetic nozzle as a new electric propulsion concept, Hoyt et al.[18], analyzed minimized anode fall potential due to a magnetic nozzle in a coaxial plasma accelerator, Zhugzhada and Nakariakov[19] explained latent heating of coronal loops due to nonlinear slow body waves generated through a laval magnetic nozzle, and Schoenberg et al.[20], presented the mechanism of plasma acceleration through a mag-

netic nozzle from MHD point of view. In 1993, Hooper[10] showed the significant constraints for plasma detachment and characterized a possible plasma detachment due to large Larmor radius effects and an ambipolar drift of a two-fluid plasma across magnetic field. In experimental research, Black et al.[21], measured a magnetic field configuration through a coaxial thruster and compared it with a one-dimensional MHD model. Furthermore, Black et al.[22], observed current sheet propagation as the evidence of an ionizing shock front due to interactions between plasma and applied magnetic field. Regarding numerical simulations, Rederick et al.[23], investigated hydromagnetic Rayleigh-Taylor instability via two-dimensional MHD simulations including unsteady flow from a magnetic nozzle. Nakashima et al.[24]a, numerically examined plasma instability in a magnetic nozzle via three-dimensional hybrid code.

After 2000, non-ideal effects in MHD theory (e.g., resistive collisions, Hall effect, and inertia effect) were examined to consider more realistic physics and plasma detachment through a magnetic nozzle. Gerwin[25] summarized those non-ideal effects theoretically through a converging-diverging magnetic nozzle. Arefiev and Breizman discussed kinetic effects[26] and analyzed ambipolar ion acceleration due to an existence of sheath at the wall[27]. As the numerical research, Mikelides et al., investigated the performance of ManetoPlasmaDynamic (MPD) thruster via MACH 2 code[30], and successfully conducted numerical simulations to identify non-ideal effects through a magnetic nozzle[31]. Inutake et al.[33], also numerically confirmed the improved efficiency of MPD arcjet by using a magnetic nozzle. Kajimura et al.[36][37][38], used three-dimensional hybrid code to control thrust vector through a magnetic nozzle in a laser fusion rocket, and improved its thrust efficiency. Sefkow and Choen[76] contributed to develop three-dimensional Particle-In-Cell (PIC) code to study electrostatic layers. To verify interactions between plasma and magnetic field, and advantages of using a magnetic nozzle, high power MPD thruster were built with a magnetic nozzle, and tested by Gilland et al[39][40]. Tobari et al.[41], evaluated diamagnetic effect of the high-beta plasma in MPD arcjet. They confirmed improved efficiency and thrust via energy conversion

through a magnetic nozzle. As other electric propulsion thruster, Choi et al.[42], developed and tested KBSI-KAIST-Hanyang (K2H) and Diversified Plasma Simulator (DiPS). Brainerd and Reisz[43] also built and tested electrodeless experimental electric thruster. In addition, Winglee et al.[44], designed and tested High Power Helicon thruster (HPH) with a magnetic nozzle both experimental and numerical ways.

On the other hand, VASIMR research has became a strong candidate for future electric propulsion since the 2000s. An overview for VASIMR engine is reported by Chang Diaz[7]. Chavers et al.[45], designed and tested momentum and heat flux sensors for VASIMR experimental research. Inutake et al.[34][35][32], examined the magnetic-laval-nozzle effect in MPD arcjet and characteristics of Ion Cyclotron Radio-Frequency (ICRF) heated ion flow. Ando et al.[46], also did some experiments to investigate a performance of ICRF Heating with a magnetic nozzle. As a numerical approach, Vecchi et al.[47], developed and tested a numerical tool to study RF-plasma interactions. Through those research, plasma should attach on magnetic flux contours to be generated and accelerated more efficiently via helicon wave and ion cyclotron heating wave. Nevertheless, plasma should eventually detach from magnetic flux contours to produce net thrust. Thereby, plasma detachment research also became an active research topic. Arefiev and Breizman[28][29] mentioned plasma detachment occurs when super-Alfvénic plasma flow stretches magnetic field to infinity. Schmit and Fisch[48] developed Hooper's plasma detachment model[10] including azimuthal velocity and analyzed plasma detachment via ambipolar electric field. Gesto et al.[49], numerically showed plasma detachment occurs if the curvature of the ion reaches to zero due to neutralizations through current free double layer in Helicon Double Layer Thruster (HDLT). Kawabuchi et al.[50], indicated a possibility of plasma detachment via ambipolar electric field by using a fully 2D3V electromagnetic PIC (TRISTAN) code. Breizman et al.[51], extended their super-Alfvénic plasma flow detachment model[28][29] by developing a Lagrangian code. As experimental proofs, West et al.[52], confirmed non-magnetized ions in HDLT exhaust and Deline et al.[53], observed super-Alfv'enic plasma flow deviated from applied magnetic field.

In recent, the magnetic nozzle effect is continuously investigated by theoretically, numerically, and experimentally. Andreussi and Pegoraro[54] adopted Hamiltonian formulation for MHD model to analyze general features of plasma acceleration through a magnetic nozzle. Ahedo and Navarro-Cavalle[55] analyzed a thermodynamic behavior to obtain better thrust efficiency. Takahashi et al.[59], examined a theoretical limit for axial momentum increase as strength of magnetic field increases due to an inhibition of a cross-field plasma diffusion. Lorzel and Mikellides[63] developed time-dependent three-dimensional MACH3 code to investigate resistive effect. Ahedo and Merino[56][65][64] computed Hall current, pressure, electric and magnetic forces contributing to thrust by using two-dimensional DIMAGNO code.Su and Shaing[67] numerically modeled a formation of current-free double layer through a magnetic nozzle. Tang et al.[68][69], developed two-dimensional axisymmetric PIC code to analyze a performance of MPD thruster with a magnetic nozzle. Singh et al.[70], simulated plasma wave effects generated by radial plasma plume. Bering et al.[71], improved an ICH coupler efficiency through a magnetic nozzle. Longmier et al.[72], verified an existence of ambipolar ion acceleration in VASIMR VX-200i device. Sheehan et al.[73], also investigated ambipolar ion acceleration in VASIMR VX-200 engine. Wiebold et al.[74][75], measured ion acceleration in the Madison Helicon eXperiment (MadHex) through current free double layer. Takahashi et al., evaluated the performance of helicon and MPD combined thruster[60][61][62] and confirmed inhibited cross-field plasma diffusion in the thruster[59]. As for plasma detachment, Ahedo and Merino[57][58][66] suggested and investigated three possible plasma detachment mechanisms (via resistivity, via electron inertia, and via induced magnetic field). As one of the most detailed and recent experimental research on plasma detachment, Olsen et al.[5], investigated plasma detachment observed in VASIMR VX-200 device. I will introduce details of their research in section 3.

Chapter 3

PLASMA DETACHMENT OBSERVED IN VASIMR RESEARCH

As one of the most recent studies on plasma detachment through a magnetic nozzle, C.S. Olsen et al.[5], observed and investigated plasma detachment in VAriable Specific Impulse Magneto-plasma Rocket (VASIMR) VX-200 engine. In their article, they showed three key indications for plasma detachment. At first, they indicated that ion flux contours detached from magnetic flux ones. Second key indication was that ion velocity was not parallel to magnetic field around the plume edge, which means ions became unmagnetized at larger radial locations in cylindrical coordinates. Lastly, they observed high-frequency electric field between detached ions and attached electrons on a magnetic flux contour. In this section, I will introduce the details of their experimental investigations, and I will analyze their results via canonical field theory in section 4.

3.1 Experimental Setup

3.1.1 VASIMR VX-200 Engine

"The VASIMR engine is a high-power, radio frequency-driven magnetoplasma rocket, capable of exhaust modulation at constant power"[7]. The first research on VASIMR engine was began at the Charles Stark Draper Laboratory and the Massachusetts Institute of Technology (MIT) in late 1970s and became more popular during 2000s. Recently, C.S. Olsen et al.[5], designed and built VASIMR VX-200 engine to investigate its performance and plasma detachment from a magnetic nozzle. "The VX-200 (VASIMR experimental-200kW) device

is a laboratory prototype operating from 2009 to 2012 demonstrating high-power densities ($6MW/m^2$ across the exit area), specific impulse ranging between 2000 and $5000s$, and thrust up to $6N$"[5].The main components of VX-200 engine shown in Fig. 3.1 are helicon wave plasma source for Argon propellant, experimental super-conducting magnets producing a magnetic nozzle, and Ion Cyclotron Heating (ICH) device which energizes ions.

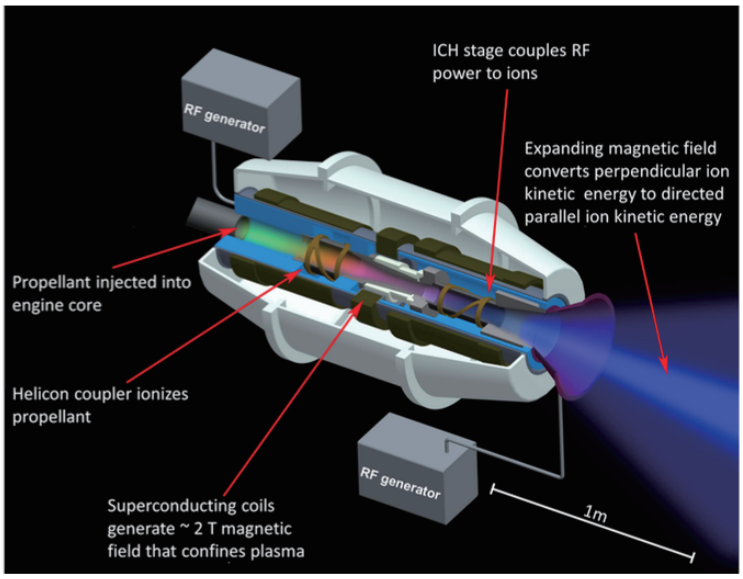

Figure 3.1: Conceptual schematic of VASIMR VX-200 engine[5]

3.1.2 Plasma Diagnostics

To measure plasma properties adequately, various plasma diagnostic devices shown in Fig. 3.2 were used in their experiments. From left to right, they had Retarding Potential Analyzer (RPA), High-Frequency (HF) electric field probe (recessed), backup plasma momentum flux sensor (PMFS), primary PMFS, 3-axis magnetometer, guard-ring Langmuir probe, azimuthal flux probe, lower ion flux probe array, and upper ion flux probe array. The detailed descriptions for each diagnostic devices can be seen in their article[5].

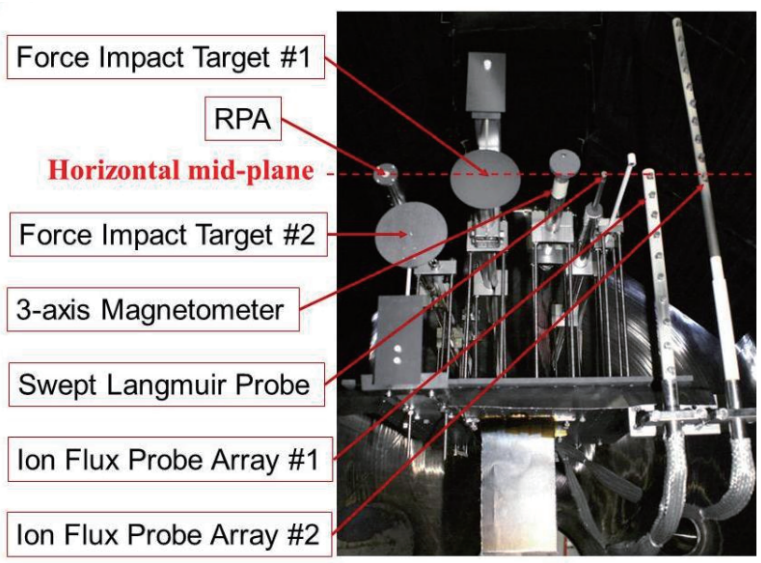

Figure 3.2: Image of plasma diagnostics[5]

3.2 Experimental Results and Discussion

3.2.1 Comparison between Ion Flux Contour and Magnetic Flux Contour

As an initial approach to verify plasma detachment, they compared ion flux contour lines with magnetic flux ones. A typical experimental schematic, Fig. 3.3, shows a convergent detachment of spatially integrated ion flux contour from magnetic flux one measured through magnetic nozzle. "The process for the investigation begins with the continuity equation under the assumption that charge sources and losses are negligible and that the flow is in steady state"[5]

$$\frac{\partial \rho}{\partial t} + \nabla \cdot (\rho \bar{u}) = S - L \ = 0 \tag{3.1}$$

They also stated that

"This form of the continuity equation is valid based on the steady mass flow rate shown in Fig. 3.4 and losses being minimized due to lower background pressures and interaction cross sections. The sources term is also presumed negligible based on verification from spectral

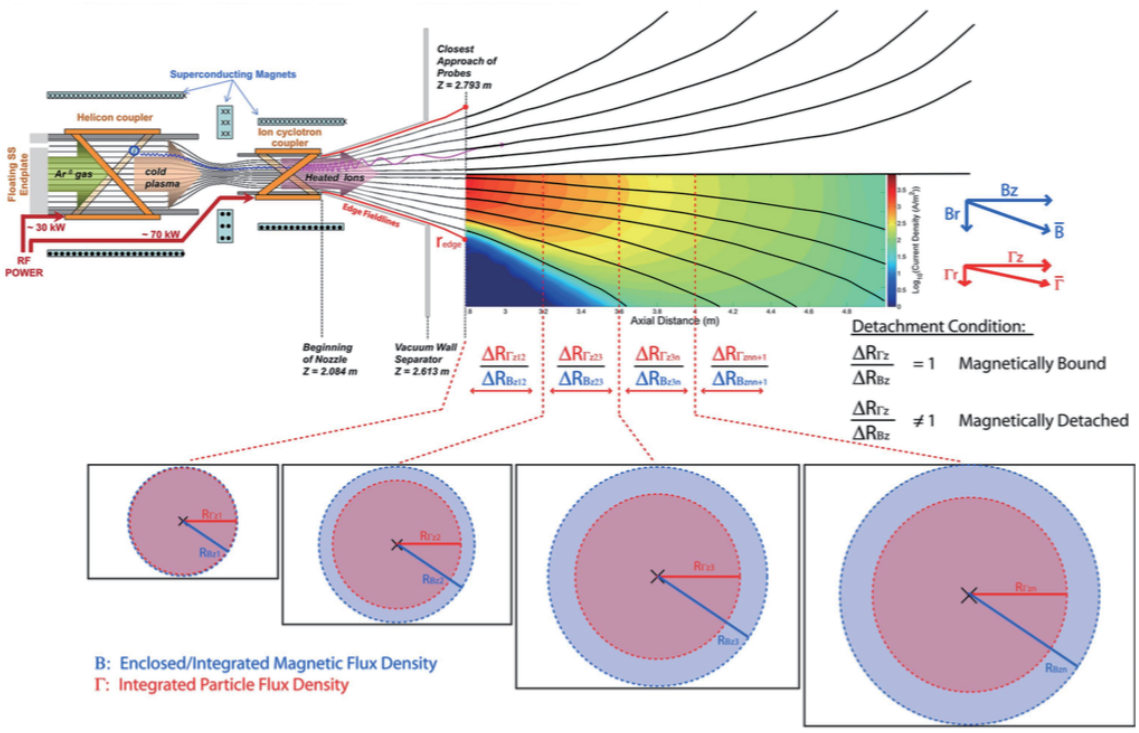

Figure 3.3: "Illustrating the method of spatially tracking lines of constant integrated ion flux and magnetic flux. Convergent detachment is shown (x-section insets) and appears as ion flux (pink) expanding slower than magnetic flux (blue)"[5].

data of a singly ionized plume, low-ion collision rate, and lack of additional external energy sources. The continuity equation permits the measurement of the plasma/magnetic flux expansion without worry of external influences."[5]

To obtain ion flux contour lines and magnetic flux ones, they numerically solved following set of operations at each axial locations where radial profile data were taken by Langmuir probe arrays facing at axial direction.

$$\Gamma_{iz}(r) = 2\pi \int_0^r J_{iz}/qrdr \tag{3.2}$$

$$f_i(r) = \frac{\Gamma_{iz}(r)}{\Gamma_{iz}(r_{edge})} \tag{3.3}$$

$$\Phi_z(r) = 2\pi \int_0^r B_z r dr \tag{3.4}$$

$$f_\Phi = \Phi_z(r_{f_i}) \tag{3.5}$$

Eq. 3.2 and 3.3 describe ion flux and ion plume fraction, f_i, which are used to map constant ion flux lines. r_{edge} is a geometric projection of the magnetic field from the inner wall shown in Fig. 3.3. Eq. 3.4 and 3.5 describe the radial magnetic flux integration and magnetic flux originally enclosing the baseline of an ion plume fraction line. To verify plasma detachment, they plotted f_i and f_Φ in Fig. 3.5 as a comparison between constant ion flux lines and constant magnetic flux ones. While they showed other results in their article for the case where only helicon plasma source was used, in this paper I particularly focus on results from the operations using both helicon source and ICH. Note that these equations are slightly different from theirs shown in their article because I found few issues in their definitions. At first, they defined magnetic flux fraction by

$$f_\Phi(r) = \frac{\Phi_z(r)}{\Phi_{0z}(r_{f_i})} \tag{3.6}$$

However, if they used their definition adequetly, their magnetic flux fraction lines would not match with their black dashed lines shown in Fig. 3.5. For example, when they mapped $f_\Phi(r) = 90\%$ line, their f_Φ line would indicate 90% of magnetic flux starting from the baseline

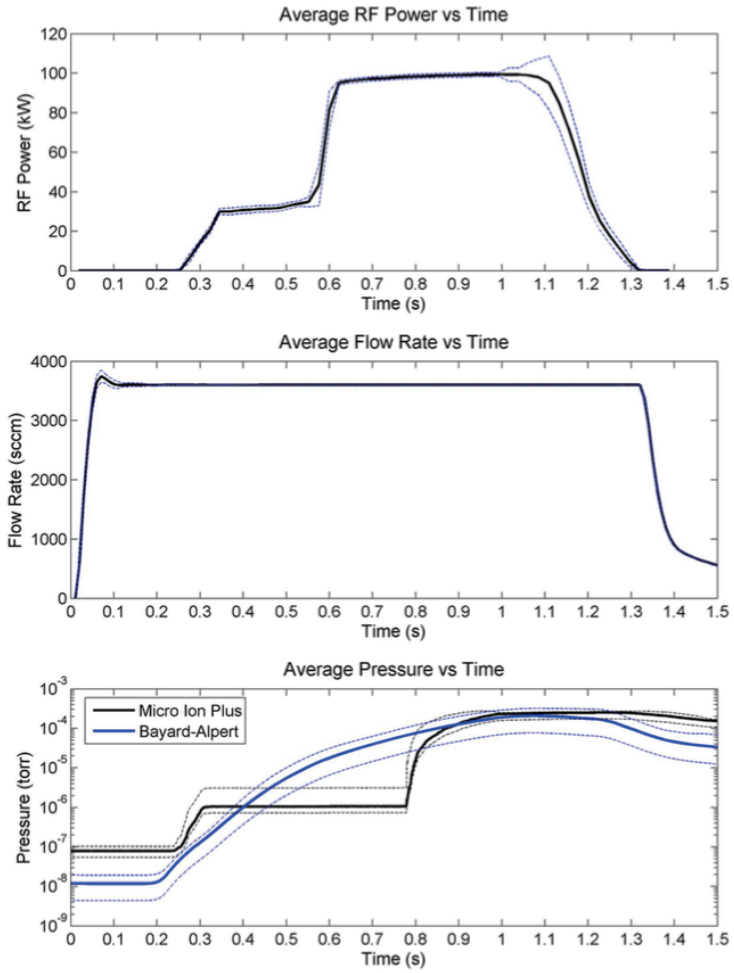

Figure 3.4: "Standard shot configuration including uncertainty bounds (dashed lines). Data analysis windows for the low- and high-power configurations were taken from 0.4 − 0.5 and 0.65 − 0.75 s, respectively. Top: average RF forward power profile. Middle: steady 3600-sccm (~ 107 mg/s) argon flow. Bottom: exhaust region chamber pressure measured by separate hot cathode ion gauges."[5]

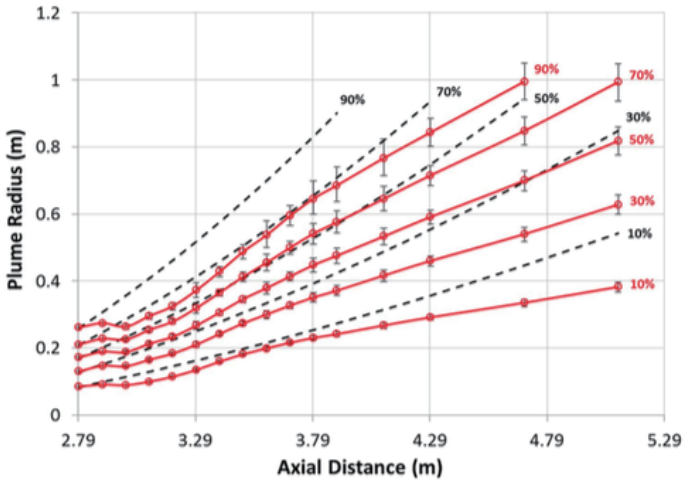

Figure 3.5: Lines of constant f_i (red solid) during the helicon + ICH operation compared with lines of constant enclosed magnetic flux (black dashed)[5]

of 90% ion plume fraction line, which means that their f_Φ line could not enclose the baseline of 90% ion plume fraction line. That f_Φ line would rather be inside of that baseline and this would contradict with their statement. Therefore, their definition of f_Φ expressed by Eq. 3.6 should be revised by Eq. 3.5.

In addition, they defined f_i as

$$f_i(r) = \frac{\Gamma_{iz}(r)}{\Gamma_{0z}(r_{edge})} \tag{3.7}$$

However, since they did not define $\Gamma_{0z}(r_{edge})$, I believe the denominator should be $\Gamma_{iz}(r_{edge})$. Indeed, the co-author J. P. Squire et al.[6], defined f_i by using Eq. 3.3 to investigate plasma detachment in their paper where C.S. Olsen was the second author. Nevertheless, just in case, I tried to find f_i numerically fitting with their f_i by using Eq. 3.7 in B where I assumed that they solved $\Gamma_{0z}(r_{edge})$ only at the baseline ($z = 2.79\,[m]$), not at each axial positions. As a result, I obtained non-realistic results and those results indeed contradicted with their statement such as they obtained collimated flow comparing with magnetic flux lines. Thereby, I re-write Eq. 3.7 into Eq. 3.3. This modification for the reference ion flux

$\Gamma_{0z}\left(r_{edge}\right)$ will indeed bring a serious issue to their statement.

From Fig. 3.5, they concluded that the separation between ion plume fraction lines and magnetic flux lines indicated the separation between ion flux contours and magnetic flux contours originally enclosing the ion plume fraction lines. However, since they plotted constant f_i lines instead of constant $\Gamma_{iz}\left(r\right)$ lines, their statement could be valid only when the denominator $\Gamma_{iz}\left(r_{edge}\right)$ is constant. For example, when $f_i = const$ and the denominator $\Gamma_{iz}\left(r_{edge}\right)$ is not constant, the numerator $\Gamma_{iz}\left(r\right)$ cannot become constant neither. One possible case that satisfies this example can be seen in Fig. 3.6. In their experiments, since they

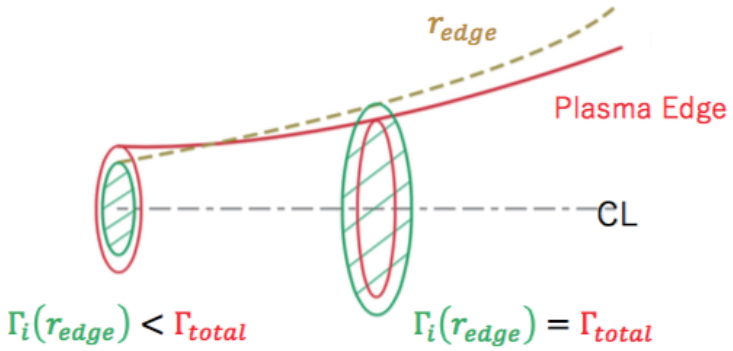

Figure 3.6: Possible shapes of plasma plume and r_{edge}

defined r_{edge} as a magnetic field line, it does not have to fit with the plasma plume edge line after leaving the physical inner wall. Thus, $\Gamma_{iz}\left(r_{edge}\right)$ is not necessarily constant throughout magnetic nozzle. Consequently, I can state that the deviations of f_i lines from magnetic flux ones did not always indicate the deviations of constant ion flux $\Gamma_{iz}\left(r\right)$ lines from magnetic flux ones. In other words, their first key indication of plasma detachment such as ion flux contours detached from magnetic flux ones is not necessarily correct.

3.2.2 Ion Unmagnetization

As the second key indication of plasma detachment, they compared ion velocity vectors with magnetic field ones by using RPA data. Contour plots of an ion velocity distribution function as a function of radial and axial ion velocity with a local magnetic field vector are shown in Fig. 3.7. They stated that "If the ions were magnetized much of the distribution

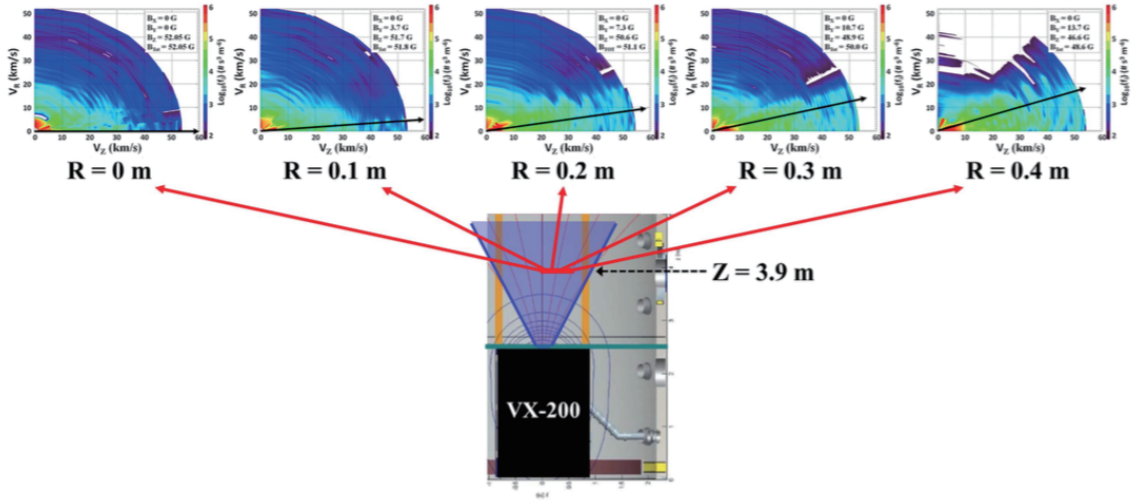

Figure 3.7: Contour maps of the ion velocity distribution function as a function of v_r and v_z at five radial locations and $z = 3.9\,[m]$. "The local magnetic field vector is overlain in each plot (black arrow)"[5]

would be expected to be more preferentially organized near the angle of the magnetic field vector"[5]. In fact, at the larger radial positions where the field has begun to curve away, axial component of ion velocity seemed to be more dominant comparing with magnetic field vector. This result was the proof of ion unmagnetization and became the second key indication of plasma detachment.

3.2.3 Existence of High-frequency Electric Field

As the third key indication, they observed high-frequency electric field, especially around the plume edge, due to loss of adiabaticity. According to [9], the breakdown of loss of adiabaticity occurs when the change in Larmor radius becomes comparable with itself.

$$\frac{\Delta r_{Li}}{r_{Li}} = \frac{\Delta \Omega_{ci}}{\Omega_{ci}} = \frac{\nu_i}{\Omega_{ci}} \frac{|\nabla B|}{B} = 1 \tag{3.8}$$

In their experiments, the breakdown for ions occurred at the green dashed line in Fig. 3.8, while electrons did not lose their adiabaticity over the entire measurement region. After

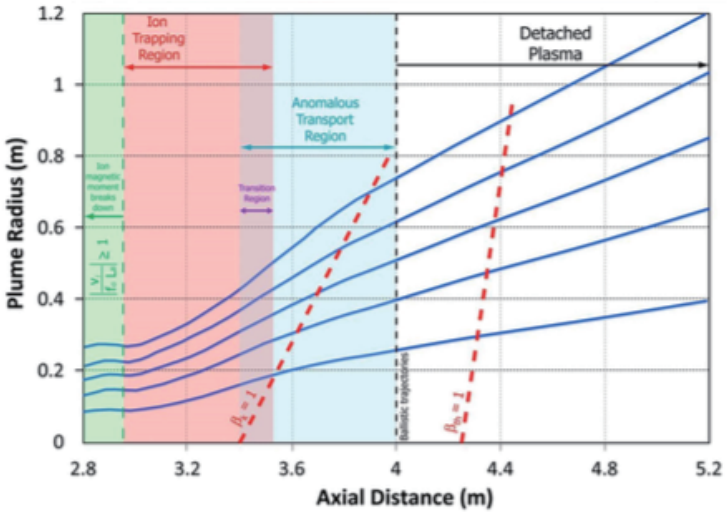

Figure 3.8: "Image summarizing various regions associated with detachment process. The flow lines (blue) are based on the integrated ion flux fraction and extended out along the linear region. Lines showing the transition above unity for kinetic and thermal beta are displayed for reference (red dashed)"[5]

losing adiabaticity, plasma entered the ion trapping region. In this region, perturbed high-frequency electric field appeared between unmagnetized ions and magnetized electrons. This electric field worked as $\vec{E} \times \vec{B}$ force and that force produced diamagnetic current. Then, $\vec{J} \times \vec{B}$ force eventually worked as centrifugal force on ions. In particular, since magnetic field

was still strong around the nozzle exit, the centrifugal force was dominant comparing with electrostatic force; hence ions seemed to be trapped.

On the other hand, as magnetic field was weakened, the fluctuating electrostatic force became dominant and plasma entered the anomalous transport region. In this region, effective collision rate for interparticle collisions was increased, and then effective resistivity became anomalous resistivity [5],[56],[10],[11]. In consequence, the tug-of-war between electrostatic force and centrifugal force enabled plasma to transport anomalously across magnetic field.

Beyond the anomalous transport region, the ions' trajectories became linear and the fluctuating electric fields were dissipated. However, since electrons were still magnetized, I believe that anomalous transport and fluctuating electric fields should still exist in the ballistical detached plasma region. Regarding this point, they mentioned that

"Although not directly observed, anomalous transport may still be occurring in the weak magnetic field regions beyond the limits of the translation stage. It may be the focus of future experiments to explore the plume further out in radius during plasma operation at lower ion energy." [5]

3.3 Summary of VASIMR VX-200 Research

In summary, they observed three key indications of plasma detachment. At first, they showed ion detachment from a magnetic flux contour, although it was not necessarily correct. Next, they indicated ion unmagnetization at larger radial positions. Lastly, they observed the existence of high-frequency electric field between magnetized electrons and unmagnetized ions due to loss of adiabaticity.

Chapter 4

CANONICAL FIELD THEORY

To investigate the plasma detachment described in section 3, I will apply canonical field theory formalized by You [1], [2], [3]. In general, interactions between plasma flow and electromagnetic field produce additional complexities and difficulties like non-ideal effects seen in MHD theory (e.g., resistive collisions, Hall effect, inertia effect, pressure gradient and pressure tensor). Around a plasma plume edge, density gradient might produce kinetic effects which cannot be investigated via fluid regime. To reduce those complexities and cost for investigations, most of analyses and numerical simulations do not include those realistic effects.

Whereas, You formalized canonical field theory from the most fundamental point-of-view using generalized Lagrangian-Hamiltonian formalism for dynamics of single particle, kinetic and fluid regimes[3]. As one of the biggest advantages of using canonical field theory, it allows us to consider more fundamental plasma physics including non-ideal and even non-fluid-regime effects. Moreover, it has one-to-one relationship with MHD theory. For example, there exist one-to-one relationships between canonical vorticity field $\vec{\Omega}_\sigma$ and magnetic field $\vec{B}$, between canonical force field $\vec{\Sigma}_\sigma$ and electric field $\vec{E}$, and between general enthalpy h_σ and some of plasma energy (e.g., kinetic energy, electrostatic potential energy, and pressure energy). Using these one-to-one relationships, we can simply apply conventional MHD intuition for canonical field theory.

4.1 Governing Equations

In this section, I will introduce governing equations in canonical field theory. Whole detailed derivations are shown in [3]. First and foremost, let me define canonical momentum $\vec{P}_\sigma$ for certain plasma species σ as

$$\vec{P}_\sigma \equiv n_\sigma m_\sigma \vec{u}_\sigma + n_\sigma q_\sigma \vec{A}_\sigma \tag{4.1}$$

General enthalpy is defined as

$$h_\sigma \equiv \frac{1}{2} n_\sigma m_\sigma u_\sigma^2 + n_\sigma q_\sigma \phi + \mathcal{P}_\sigma \tag{4.2}$$

Canonical vorticity field is defined by

$$\vec{\Omega}_\sigma \equiv \nabla \times \vec{P}_\sigma \tag{4.3}$$

Canonical force-field is defined by

$$\vec{\Sigma}_\sigma \equiv -\nabla h_\sigma - \frac{\partial \vec{P}_\sigma}{\partial t} \tag{4.4}$$

From generalized Lagrangian-Hamiltonian formalism, generalized form of Ohm's law (equation of motion) can be written as

$$\vec{\Sigma}_\sigma + \left(\vec{u}_\sigma \times \vec{\Omega}_\sigma \right) = \vec{R}_\sigma \tag{4.5}$$

where dissipative force $\vec{R}_\sigma$ is

$$\vec{R}_\sigma \equiv -\nabla \left(\frac{1}{2} \epsilon_\sigma \Sigma_\sigma^2 - \frac{\Omega_\sigma^2}{2\mu_\sigma} \right) \tag{4.6}$$

You[3] explained Eq. 4.6 by stating that "dissipative forces represent an incomplete conversion of canonical vorticity "potential" energy $\frac{\Omega_\sigma^2}{2\mu_\sigma}$ into canonical force-field "kinetic" energy $\frac{1}{2}\epsilon_\sigma \Sigma_\sigma^2$."

Next, let me derive generalized form of Maxwell's equations in canonical field theory. First of all, generalized Faraday's law can be derived by taking curl of canonical force field $\vec{\Sigma}_\sigma$,

$$\nabla \times \vec{\Sigma}_\sigma = -\frac{\partial \vec{\Omega}_\sigma}{\partial t} \tag{4.7}$$

Taking divergence of canonical vorticity $\vec{\Omega}_\sigma$, I can obtain generalized Gauss's law for canonical vorticity field such as

$$\nabla \cdot \vec{\Omega}_\sigma = 0 \tag{4.8}$$

Defining canonical source term $\mathbb{q}\mathbb{p}_\sigma$ for canonical force field as

$$\frac{\mathbb{q}\mathbb{p}_\sigma}{\epsilon_\sigma} \equiv \nabla \cdot \left[\vec{R}_\sigma - \left(\vec{u}_\sigma \times \vec{\Omega}_\sigma\right)\right] \tag{4.9}$$

generalized gauss's law for canonical force field can be derived as

$$\nabla \cdot \vec{\Sigma}_\sigma = \frac{\mathbb{q}\mathbb{p}_\sigma}{\epsilon_\sigma} \tag{4.10}$$

Lastly, taking curl of canonical vorticity brings us generalized Ampére's law

$$\nabla \times \vec{\Omega}_\sigma = \mu_\sigma \vec{\mathbb{J}}_\sigma + \mu_\sigma \epsilon_\sigma \frac{\partial \vec{\Sigma}_\sigma}{\partial t} \tag{4.11}$$

where canonical current density is defined as

$$\vec{\mathbb{J}}_\sigma \equiv \mathbb{q}\mathbb{p}_\sigma \vec{u}_\sigma \tag{4.12}$$

To keep gauge-invariant for canonical momentum, canonical Lorentz gauge condition can be written as

$$\nabla \cdot \vec{P}_\sigma + \mu_\sigma \epsilon_\sigma \frac{\partial h_\sigma}{\partial t} = 0 \tag{4.13}$$

In summary, all governing equations compared with MHD theory can be seen in Table 4.1 and in Table 4.2.

4.2 Frozen-in Theorem for Canonical Field Theory

Likewise ideal MHD theory, I will derive frozen-in theorem for canonical field theory. At first, canonical vorticity flux is defined as

$$\Psi_\sigma \equiv \int \vec{\Omega}_\sigma \cdot d\vec{S} \tag{4.14}$$

Table 4.1: Comparison of governing equations between MHD Theory and Canonical Field Theory

	MHD Theory	Canonical Field Theory
Ohm's law	$\vec{E}+\left(\vec{u}\times\vec{B}\right)=\vec{R}_{non-ideal}$	$\vec{\Sigma}_\sigma+\left(\vec{u}_\sigma\times\vec{\Omega}_\sigma\right)=\vec{R}_\sigma$
Faraday's law	$\nabla\times\vec{E}=-\frac{\partial\vec{B}}{\partial t}$	$\nabla\times\vec{\Sigma}_\sigma=-\frac{\partial\vec{\Omega}_\sigma}{\partial t}$
Gauss's law	$\nabla\cdot\vec{B}=0$	$\nabla\cdot\vec{\Omega}_\sigma=0$
Gauss's law	$\nabla\cdot\vec{E}=\frac{nq}{\epsilon_0}$	$\nabla\cdot\vec{\Sigma}_\sigma=\frac{\mathbb{q}\mathbb{\mu}_\sigma}{\epsilon_\sigma}$
Ampére's law	$\nabla\times\vec{B}=\mu_0\vec{J}+\frac{1}{c^2}\frac{\partial\vec{E}}{\partial t}$	$\nabla\times\vec{\Omega}_\sigma=\mu_\sigma\vec{\mathbb{J}}_\sigma+\mu_\sigma\epsilon_\sigma\frac{\partial\vec{\Sigma}_\sigma}{\partial t}$
Lorentz gauge condition	$\nabla\cdot\vec{A}+\frac{1}{c^2}\frac{\partial\phi}{\partial t}=0$	$\nabla\cdot\vec{P}_\sigma+\mu_\sigma\epsilon_\sigma\frac{\partial h_\sigma}{\partial t}=0$

Using Stokes' theorem,

$$\Psi_\sigma=\oint\vec{P}_\sigma\cdot d\vec{l}=\oint\left(n_\sigma m_\sigma\vec{u}_\sigma+n_\sigma q_\sigma\vec{A}\right)\cdot d\vec{l} \tag{4.15}$$

Using canonical Ohm's law with zero dissipative force, $\vec{R}_\sigma=0$, and canonical Faraday's law, the change in Ψ_σ in the frame moving with plasma is

$$\frac{d\Psi_\sigma}{dt}=\frac{\partial\Psi_\sigma}{\partial t}+\left(\vec{v}\cdot\nabla\right)\Psi_\sigma=\oint\left(\vec{u}-\vec{v}\right)\times\vec{\Omega}_\sigma\cdot d\vec{l}=0 \tag{4.16}$$

Therefore, I can state that canonical vorticity flux is frozen-in plasma when $\vec{R}_\sigma=0$.

From frozen-in theorem for canonical field theory, plasma flow can be controlled by obtaining appropriate shape of canonical vorticity flux tube. Considering plasma detachment, when $\vec{R}_\sigma=0$, plasma detaches from ψ contour, but attaches on Ψ_σ contour. On the other hand, when $\vec{R}_\sigma\neq0$, plasma must detach from Ψ_σ contour and could attach on ψ contour when plasma is magnetized. To understand the mechanism of plasma detachment, it is important to consider canonical vorticity flux Ψ_σ and dissipative force $\vec{R}_\sigma$.

Table 4.2: One-to-one relationships between MHD Theory and Canonical Field Theory

MHD Theory	Canonical Field Theory
$\vec{E}$	$\vec{\Sigma}_\sigma$
$nq\phi$	h_σ
$\vec{B}$	$\vec{\Omega}_\sigma$
$\vec{A}$	$\vec{P}_\sigma$
$\rho_c \equiv nq$	$\mathfrak{qu}_\sigma$
$\vec{R}_{non-ideal} \equiv \eta\vec{J} + \frac{1}{Zqn}\left(\vec{J}\times\vec{B} - \nabla P_e - \nabla\cdot\overleftrightarrow{\Pi}_e\right)$	$\vec{R}_\sigma \equiv -\nabla\left(\frac{1}{2}\epsilon_\sigma\Sigma_\sigma^2 - \frac{\Omega_\sigma^2}{2\mu_\sigma}\right)$

Chapter 5

ANALYSIS OF PLASMA DETACHMENT VIA CANONICAL FIELD THEORY

From Eq. 4.15, there are three key steps to map canonical vorticity flux Ψ_σ contour: finding vector potential $\vec{A}$, finding number density profile n_σ, and finding velocity profile $\vec{u}_\sigma$. In this section, I will present analytical fits with experimental data shown in section 3, and investigate the mechanism of plasma detachment via canonical field theory.

5.1 Constant Ion Flux Contour

5.1.1 Magnetic Field Configuration

In the experiments, the magnetic field is produced from experimental superconducting magnets. However, due to less information about those magnets (e.g., location, width, radius, and current carried) in their article, let me assume that an ideal single current loop produces magnetic field

$$A_\theta = \frac{\mu_0}{4\pi} \frac{4Ia}{\sqrt{a^2 + r^2 + z^2 + 2ar}} \left[\frac{(2 - k^2) K(k) - 2E(k)}{k^2} \right] \tag{5.1}$$

where a is a radius of a circular current loop carrying current I and the argument k of the elliptic integral is

$$k^2 = \frac{4ar}{a^2 + r^2 + z^2 + 2ar} \tag{5.2}$$

Taking curl of $\vec{A}$, I can obtain the following similar enough magnetic field configuration shown in Fig. 5.1 and Fig. 5.2. Note that there are three different experimental results in Fig. 5.1; one is for vacuum case, another one is for helicon plasma source with ICH case, the

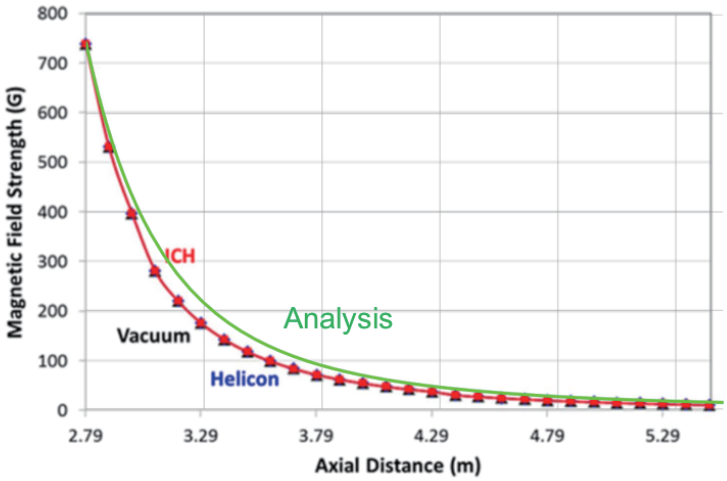

Figure 5.1: Comparison for the strength of magnetic field on z-axis for vacuum case (black), helicon only case (blue), and helicon + ICH case (red) in experiments and my analytical one (green)[5]

other one is for helicon plasma source without ICH case. Olsen et al., mentioned that these three experimental results were mostly overlapped, and the largest difference was only 2%.

5.1.2 Number Density Profile

Number density profile can be derived from current density profile measured by Langmuir probe arrays such as

$$j_{iz}(r,z) = \mathrm{e}^{-\frac{1}{2}} n_i(r,z)\, q_i c_s(z) \tag{5.3}$$

where I assumed quasineutral plasma ($n_e = n_i$). Bohm velocity $c_s(z)$ can be derived from current density and number density data measured on z-axis where I assumed radially uniform Bohm velocity because of less information about its radial profile.

$$c_s(z) = \frac{j_{iz}(0,z)}{\mathrm{e}^{-\frac{1}{2}} n_i(0,z)\, q_i} \tag{5.4}$$

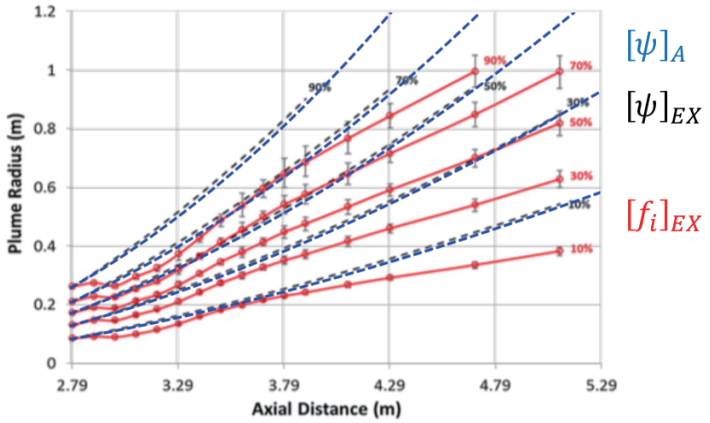

Figure 5.2: Comparison for experimental magnetic flux lines (black dashed), experimental magnetic flux fraction f_i lines (red) and my analytical magnetic flux (blue dashed)[5]

Regarding radial current density profile, I assumed Gaussian distribution $j_{iz}(r,z) \propto \mathrm{e}^{-ar^b}$ and numerically solved for ion plume fraction lines f_i fitting with experimental ones shown in Fig. 5.4. From Fig. 5.4, I can confirm that my analytical constant ion plume fraction f_i

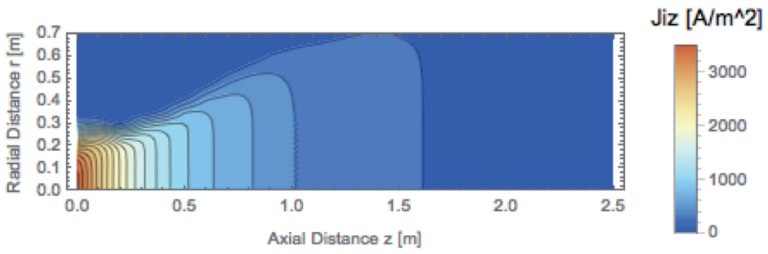

Figure 5.3: Axial ion current density contour map

lines (blue) seem to match with measured ones (red).

Plotting number density contour map with r_{edge} line (yellow dashed line) in Fig. 5.5, I can see that r_{edge} at the beginning is indeed placed inside the plume edge like I expected in Fig. 3.6. From this result, I can state that $\Gamma_i(r_{edge})$ is not necessarily constant at each

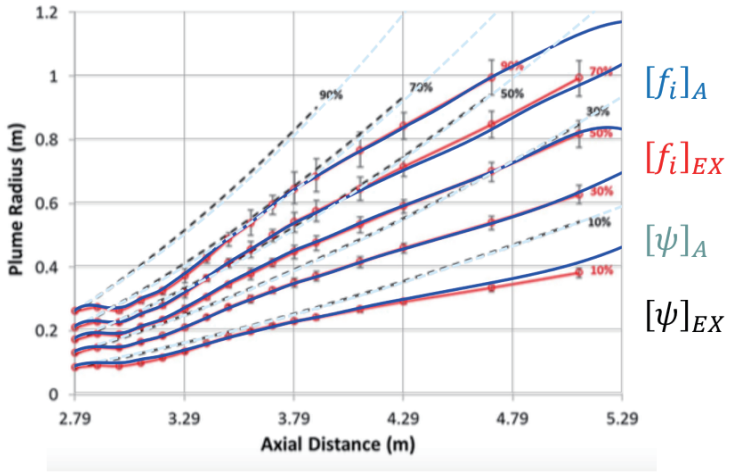

Figure 5.4: Comparison between experimental ion flux fraction f_i lines (red) and my analytical f_i lines (blue) with experimental magnetic flux ψ lines (black dashed) and analytical magnetic flux ψ lines (light blue dashed)[5]

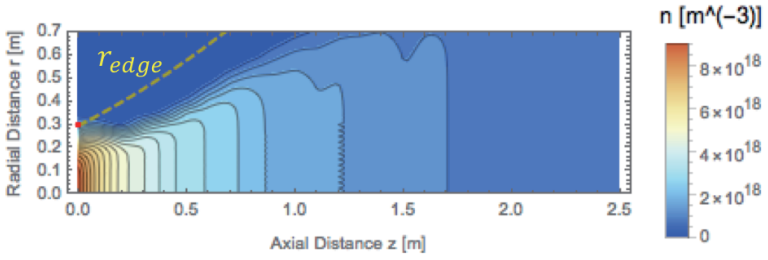

Figure 5.5: number density contour map with r_{edge} (yellow dashed). Red point indicates the basepoint of r_{edge}

axial position. In fact, calculating $\Gamma_i\left(r_{edge}\right)$, I can show non-constant $\Gamma_i\left(r_{edge}\right)$ in Fig. 5.6. As a result, I can conclude that their first key indication, "ion flux contour detached from

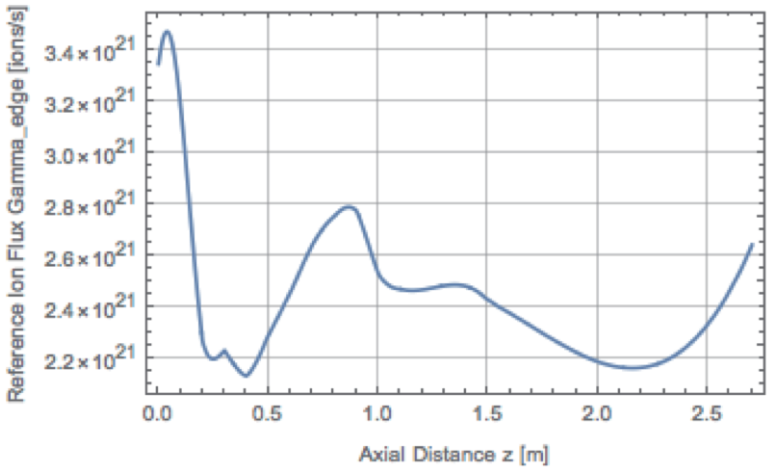

Figure 5.6: number density contour map with r_{edge} (yellow dashed). Red point indicates the basepoint of r_{edge}

magnetic flux contour" was incorrect. Plotting actual constant ion flux contour lines in Fig. 5.7, I can see that most of constant ion flux contour lines did not actually separate from magnetic flux contour ones.

On the other hand, my analytical constant ion flux $\Gamma_i\left(r\right)$ lines are consistent with their second key indication. At $z = 1.2$ in Fig. 5.7 (at $z = 3.9$ in their experiments), $\Gamma_i\left(r\right)$ lines start to separate and be collimated at larger radial positions. This result is consistent with their second indicator such that "ions became unmagnetized and collimated as r increases." As another possible counter-argument to my analysis, it can be stated that $\Gamma_i\left(r\right)$ lines might not be true constant ion flux lines because they used informal definition for ion flux. In general, ion flux should be defined as

$$\Gamma_{itrue} \equiv \int n_i \vec{u}_i \cdot d\vec{S} \tag{5.5}$$

Whereas, in their article, ion flux was defined by using current density obtained from Lang-

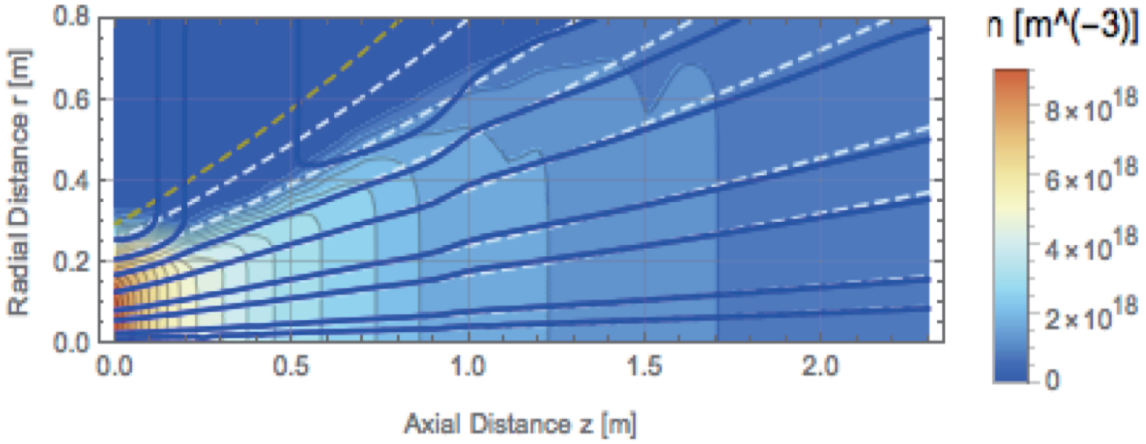

Figure 5.7: n_i contour map with constant ion flux $\Gamma_i(r)$ lines (blue solid), constant magnetic flux ψ lines (light blue dashed), and r_{edge} (yellow dashed)

muir probes

$$\Gamma_{iex} = \int e^{-\frac{1}{2}} n_\infty \vec{c}_s \cdot d\vec{S} \tag{5.6}$$

This informal definition would bring inadequate plots for ion flux contour lines. However, since my analytical $\Gamma_i(r)$ lines are consistent with their second evidence based on RPA data, at least I can state that my $\Gamma_i(r)$ lines are approximately equal to the true ones, $\Gamma_{iex} \simeq \Gamma_{itrue}$, except for the plume edge region.

5.2 Canonical Vorticity Flux Contour

5.2.1 Velocity Profile

To understand plasma detachment around the plume edge region, we need to plot canonical vorticity flux Ψ_σ contour lines. The last step to map Ψ_σ contours, I need to find velocity profile. Unfortunately, since we have less information about the radial profile of ion velocity,

let me assume electrons are fully magnetized as they stated[5],

$$\vec{u}_e \equiv u_e \frac{\vec{B}}{\left|\vec{B}\right|} = u_e \hat{b} \tag{5.7}$$

Additionally, since VASIMR VX-200 engine is electrodeless, assuming zero net plasma current,

$$\vec{j} = n_i q_i \left(\vec{u}_i - \vec{u}_e\right) = 0 \tag{5.8}$$

Then, ion velocity can be derived as

$$\vec{u}_i = \vec{u}_e = u_e \hat{b} = u_i \hat{b} \tag{5.9}$$

As a result, I can state that ions are also magnetized, otherwise my two assumptions are incorrect such that there should be net current or both ions and electrons are unmagnetized. However, since most of constant $\Gamma_i(r)$ lines attached on ψ lines in Fig. 5.7, let me use magnetized plasma velocity to plot canonical vorticity flux Ψ_σ contour map.

5.2.2 Comparison between Ion Flux Contour and Ion Canonical Vorticity Flux Contour

Ψ_i contour lines are plotted in Fig. 5.8. From this figure, I will mention five notable points. First and foremost, in the core plasma plume region, while ions are mostly magnetized, Ψ_i lines (orange) derived by using magnetized velocity did not fit with $\Gamma_i(r)$ lines (blue). On the other hand, around the plume edge region, I expected that Ψ_i lines would not fit with the plume edge line since $\Gamma_i(r)$ lines (blue) are unmagnetized; however, Ψ_i lines surprisingly fitted with the plume edge line quite well. Thirdly, there exist returning plasma flows as r increases. Before mentioning all five notable points, let me describe these three notable points in the following sections.

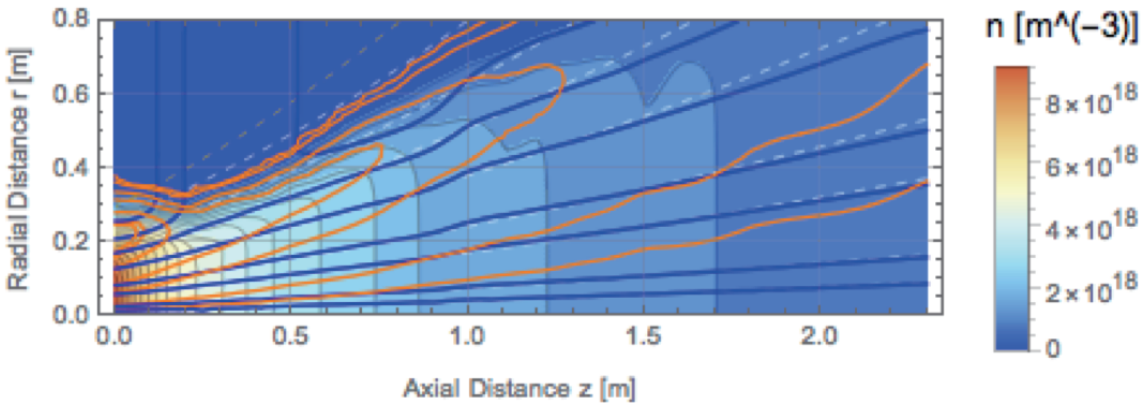

Figure 5.8: n_i contour map with constant canonical vorticity flux Ψ_i lines (orange), constant ion flux $\Gamma_i(r)$ lines (blue), constant magnetic flux ψ lines (light blue dashed), and r_{edge} (yellow dashed)

5.2.3 Dissipative Term $\vec{R}_\sigma$ makes Plasma Detach from Canonical Vorticity Flux Contour

As for the first notable point, I can simply explain by using non-zero dissipative force, $\vec{R}_\sigma \neq 0$. As I had already mentioned in section 4, when $\vec{R}_\sigma \neq 0$, plasma can detach from Ψ_σ contour. Therefore, in the core plasma plume region, non-zero dissipative force, $\vec{R}_\sigma \neq 0$, makes plasma detach from Ψ_σ lines (orange) and attach on ψ lines (light blue dashed). Thereby both ions and electrons can be magnetized.

In contrast, $\vec{R}_\sigma = 0$ force enables plasma to attach on Ψ_σ contour lines around the plume edge region. In that region, since $n_\sigma \to 0$, I can write $\vec{\Omega}_\sigma \to 0$ and $\vec{\Sigma}_\sigma \to 0$. Hence, even if we used inaccurate velocity profile to plot Ψ_σ, like magnetized velocity, canonical vorticity flux and dissipative term would become $\Psi_\sigma \to cst$ and $\vec{R}_\sigma \to 0$. As a result, I can state my analytical Ψ_i lines are approximately equal to the true ones that should be derived by using the true velocity profile around the plume edge region, and exactly same at the plume edge due to $\vec{R}_\sigma = 0$.

5.2.4 Returning Plasma Flow

The existence of returning plasma flow is guaranteed by Gauss's law for canonical vorticity field such as $\nabla \cdot \vec{\Omega}_\sigma = 0$ like a closed loop of magnetic field. However, unlike magnetic field, since $\vec{\Omega}_\sigma$ is defined by using number density n_σ, all returning paths should be enclosed by a plasma plume edge. Mathematically, these returning points appear when $\frac{\partial \Psi_\sigma}{\partial z} = 0$.

$$\frac{\partial \Psi_\sigma}{\partial z} = \oint \frac{\partial \vec{P}_\sigma}{\partial z} \cdot d\vec{l} = \oint \left[\frac{\partial n_\sigma}{\partial z} \left(m_\sigma \vec{u}_\sigma + q_\sigma \vec{A} \right) + n_\sigma \left(m_\sigma \frac{\partial \vec{u}_\sigma}{\partial z} + q_\sigma \frac{\partial \vec{A}}{\partial z} \right) \right] \cdot d\vec{l} \tag{5.10}$$

In general, $n_\sigma \to 0$ and $\frac{\partial n_\sigma}{\partial z} \to 0$ around the plume edge region. Therefore, I can infer that returning points will appear around the plume edge region.

5.2.5 Additional Notable Points

Another notable point from Fig. 5.8 is that ion flux $\Gamma_i(r)$ lines around the nozzle exit separate from Ψ_σ lines and diverge to infinity. In my opinion, since Olsen et al., measured the current density by using $-z$ directed Langmuir probes, they could not measure returning plasma flow appropriately. For this reason, ion flux $\Gamma_i(r)$ lines around the nozzle exit seem to diverge to infinity.

Regarding the high-frequency electric field, I can explain the existence and dissipation of this electric field by considering canonical vorticity flux for ions Ψ_i and for electrons Ψ_e. In the core plume region, since both ions and electrons are magnetized, it is difficult to observe electric field. In fact, the author stated that the strength of electric field was larger as r increases. Around the plume edge region, since $\vec{R}_\sigma \simeq 0$, both ions and electrons try to re-attach on their own canonical vorticity flux Ψ_σ contours. Then, when constant Ψ_i lines do not match with constant Ψ_e lines, electric field appears, vice versa. Considering canonical vorticity flux for each species, the biggest difference can be seen in their inertia terms.

$$\Psi_i = \oint \left(n_i m_i \vec{u}_i + n_i q_i \vec{A} \right) \cdot d\vec{l} \tag{5.11}$$

$$\Psi_e = \oint \left(n_e m_e \vec{u}_e + n_e q_e \vec{A} \right) \cdot d\vec{l} \tag{5.12}$$

Around the nozzle exit, since the inertia effects for each species are not negligible, constant Ψ_i lines deviate from constant Ψ_e lines. In contrast, since number density becomes much smaller at the far downstream region than that around the nozzle exit, those inertia effects can become negligible. As a result, high-frequency electric field can be dissipated. This explanation is consistent with their third key indication such that they observed strong perturbed electric field around the plume edge and it dissipated as z increases.

5.3 Summary of Analysis

I confirmed that my analytical results via canonical field theory are consistent with two of three key indications observed in VASIMR experimental research. At first, their first key indication becomes incorrect now because $\Gamma_i \left(r_{edge} \right)$ is actually not constant, and constant ion flux lines did not actually separate from magnetic flux ones. Secondly, my analytical ion flux $\Gamma_i \left(r \right)$ lines showed the consistent result with their second key indication, namely analytical $\Gamma_i \left(r \right)$ lines are also deviated and collimated at larger radial positions. Lastly, while electrons are neither fully magnetized around the plume edge region because of $\vec{R}_\sigma \simeq 0$, I can explain the existence of high-frequency electric field by considering deviations between Ψ_i lines and Ψ_e lines. Also, the dissipation of the electric field at larger axial locations can be explained by matching of Ψ_i lines and Ψ_e ones.

The transitions of dissipative force and the mechanism of plasma detachment through magnetic nozzle are summarized in Fig. 5.9.

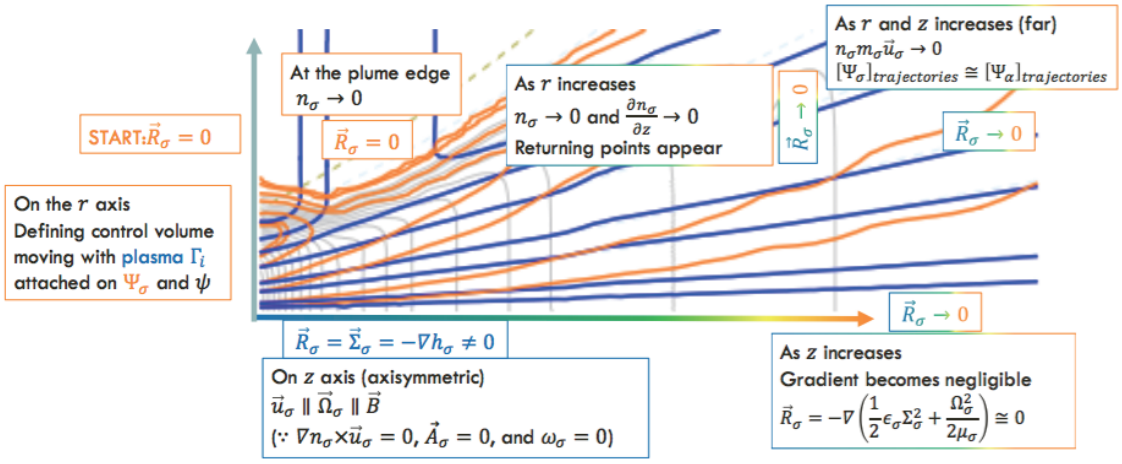

Figure 5.9: Summary of plasma detachment via canonical force field theory

Chapter 6

SUMMARY

In this paper, I have investigated the mechanism of plasma detachment through magnetic nozzle via canonical field theory. As one of the most recent experimental proofs, Olsen et al[5]., observed and investigated plasma detachment through magnetic nozzle in VASIMR VX-200 engine. In their article, they observed three key indications of plasma detachment; constant ion flux lines deviated from constant magnetic flux ones; ions became unmagnetized at larger radial locations; high-frequency electric field appeared and dissipated as z increases. However, since I found some issues in their definitions, in particular their calculations for the reference ion flux $\Gamma_i\left(r_{edge}\right)$, their first key indication becomes incorrect now. After solving for numerical fits with their experimental results, I found that constant ion flux $\Gamma_i\left(r\right)$ lines did not actually separate from constant magnetic flux ones. Whereas, my analytical results are consistent with the other two key indications. My analytical constant ion flux $\Gamma_i\left(r\right)$ lines are collimated and deviated from magnetic flux ones as r increases. In addition, their third key indication can be explained by considering the separation between canonical vorticity flux contours for each ions and electrons.

To explain the mechanism of plasma detachment, I utilized frozen-in theorem in canonical field theory likewise ideal MHD theory; canonical vorticity flux is frozen-in plasma when dissipative force $\vec{R}_\sigma = 0$. At the beginning, plasma detached from canonical vorticity flux Ψ_σ contours due to non-zero dissipative force $\vec{R}_\sigma \neq 0$ and could attache on rather magnetic flux lines. However, since number density n_σ decreases as r increases, dissipative force is getting close to zero. As a result, $\vec{R}_\sigma \simeq 0$ force makes plasma re-attach on canonical vorticity flux Ψ_σ contours. Also, at the quite far downstream region from magnetic nozzle, since most

of plasma parameters become approximately uniform, $\vec{R}_\sigma \equiv -\nabla\left(\frac{1}{2}\epsilon_\sigma\Sigma_\sigma^2 - \frac{\Omega_\sigma^2}{2\mu_\sigma}\right) \simeq 0$ and plasma try to re-attach on Ψ_σ contour.

Another notable point for Ψ_σ contour is the existence of returning plasma flow. Likewise magnetic field, since canonical vorticity field $\vec{\Omega}_\sigma$ also satisfies Gauss's law, $\vec{\Omega}_\sigma$ should have a closed loop trajectory. On the other hand, unlike magnetic field, since $\vec{\Omega}_\sigma$ is defined by using n_σ, all returning paths should be enclosed by a plasma plume edge. Therefore, as n_σ and axial gradient of number density $\frac{\partial n_\sigma}{\partial z}$ decrease and get close to zero at larger radial positions, plasma should re-attach on Ψ_σ lines and eventually returns to the nozzle.

Meanwhile, constant Ψ_i lines do not have to match with constant Ψ_e lines even around the plume edge region. In particular, around the nozzle exit, since inertia effects cannot be negligible, the deviations of each Ψ_σ trajectories generate high-frequency electric field around the plume edge region. At the far downstream region, by contrast, since n_σ decreases through diverging magnetic nozzle, inertia effects become negligible and Ψ_σ trajectories for each species match with one another. Eventually, electric field between ions and electrons dissipates at the far downstream region. This is consistent with their third key indication observed in the VASIMR experiment.

In conclusion, canonical field theory can explain the mechanism of plasma detachment by considering canonical vorticity flux contour and a transition of dissipative force. The analyses via canonical field theory are mostly consistent with VASIMR VX-200 experimental results. To verify the existence of the returning plasma flow, I suggest to use Mach probes instead of using Langmuir probes. Also, it is necessary to plot true canonical vorticity flux contour by using true velocity profile obtained from Mach probes or RPA arrays. For more practical purposes, it is also quite important to investigate the dynamics of canonical vorticity flux tube for analyzing plasma detachment and a formation of returning plasma flow through a plasma jet.

Appendix A

FROZEN-IN THEOREM

Frozen-in theorem in ideal MHD theory is derived based on

$$\frac{d\psi}{dt} = 0 \tag{A.1}$$

Using Eq. 2.1,

$$\frac{d\psi}{dt} = \int \frac{d\vec{B}}{dt} \cdot d\vec{S} + \int \vec{B} \cdot \frac{d\Delta\vec{S}}{dt} \tag{A.2}$$

The first term becomes

$$\int \frac{d\vec{B}}{dt} \cdot d\vec{S} = \lim_{\delta t \to 0} \int \frac{\vec{B}\left(t+\delta t\right) - \vec{B}\left(t\right)}{\delta t} \cdot d\vec{S} = \int \frac{\partial \vec{B}\left(t\right)}{\partial t} \cdot d\vec{S} \tag{A.3}$$

Using Faraday's law and Ohm's law,

$$\int \frac{\partial \vec{B}\left(t\right)}{\partial t} \cdot d\vec{S} = \int \nabla \times \left(\vec{u} \times \vec{B}\right) \cdot d\vec{S} \tag{A.4}$$

Using Stokes' theorem,

$$\int \nabla \times \left(\vec{u} \times \vec{B}\right) \cdot d\vec{S} = \oint \left(\vec{u} \times \vec{B}\right) \cdot d\vec{l} \tag{A.5}$$

The second term is

$$\int \vec{B} \cdot \frac{d\Delta\vec{S}}{dt} = \int \vec{B} \cdot \frac{\vec{u}dt \times \Delta\vec{l}}{dt} = \int \vec{B} \cdot \left(\vec{u} \times \Delta\vec{l}\right) \tag{A.6}$$

From Eq. A.5 and A.6, these two terms are cancelled out one another by considering triple scalar product. Therefore, I can derived Eq. A.1.

Appendix B

CONSTANT $\Gamma_{IZ}\left(R_{EDGE}\right)$ CASE

Likewise section 5.1.2, let me find f_i numerically fitting with experimental data. Assuming that they solved $\Gamma_{0z}\left(r_{edge}\right)$ only at the baseline ($z = 2.79\,[m]$), I can plot current density, ion fraction lines, and number density in Fig. B.1, B.2, and B.3 where I assumed radial current density profile as Gaussian distribution.

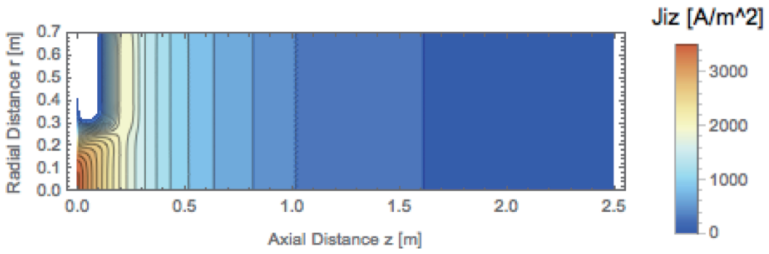

Figure B.1: Axial ion current density contour map

From these figures, I could not find the best numerical fit with experimental data. Also, I can state that these results are unrealistic and contradicts with their statement that they obtained collimated plasma plume. As one possible case, the current density distribution could not look like Gaussian distribution. For example, plasma could have a shear flow.

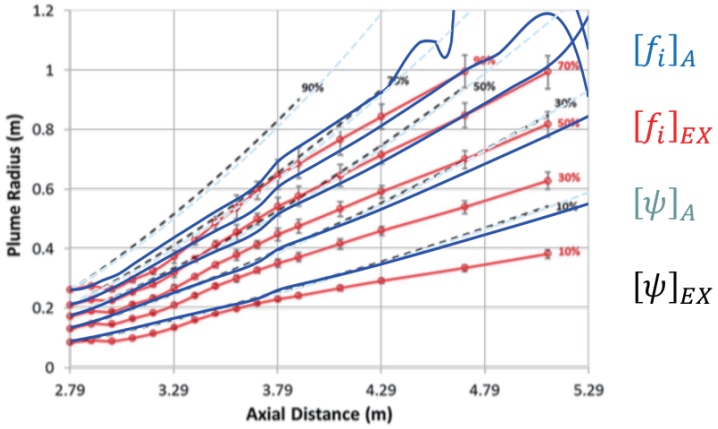

Figure B.2: Comparison between experimental ion flux fraction f_i lines (red) and my analytical f_i lines (blue) with experimental magnetic flux ψ lines (black dashed) and analytical magnetic flux ψ lines (light blue dashed)[5]

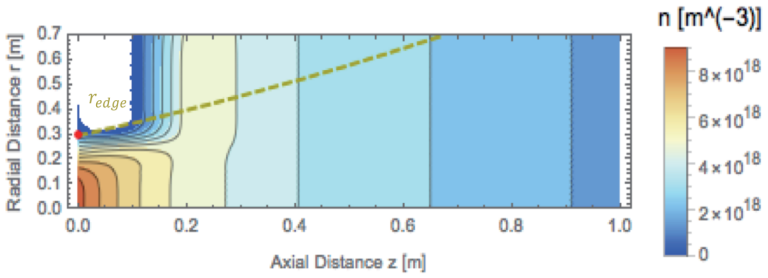

Figure B.3: number density contour map with r_{edge} (yellow dashed). Red point indicates the basepoint of r_{edge}

BIBLIOGRAPHY

[1] S. You, "The Transport of Relative Canonical Helicity," *Physics of Plasma*, vol. 19, Sep. 2012, doi: 10.1063/1.4752215

[2] S. You, "A Two-fluid Helicity Transport Model for Flux-rope Merging," *Plasma Physics and Controlled Fusion*, vol. 56, Mar. 2014, doi: 10.1088/0741-3335/56/6/064007

[3] S. You, "A Field Theory Approach to the Evolution of Canonical Helicity and Energy," *Physics of Plasma*, vol. 23, Jul. 2016, doi: 10.1063/1.4956465

[4] E. S. Lavine and S. You, "The Topology of Canonical Flux Tubes in Flared Jet Geometry," *The Astrophysical Journal*, 835:89 (pp18), Jan. 2017, doi: 10.3847/1538-4357/835/1/89

[5] C.S. Olsen et al., "Investigation of Plasma Detachment From a Magnetic Nozzle in the Plume of the VX-200 Magnetoplasma Thruster," *IEEE Transactions on Plasma Science*, vol. 43(1), Jan. 2015.

[6] J. P. Squire et al., "VASIMR VX-200 Operation at 200 kW and Plume Measurements: Future Plans and an ISS EP Test Platform," *The 32nd International Electric Propulsion Conference*, 2011

[7] F.R. Chang Diaz, "An Overview of the VASIMR Engine: High Power Space Propulsion with RF Plasma Generation and Heating," *American Institute of Physics*, Conference Proceeding 595, 2001.

[8] F. Richard, "Plasma Physics: an Introduction by Richard Fitzpatrick," *Contemporary Physics*, vol. 57(4), p.606, doi: 10.1080/00107514.2016.1217047

[9] M. D. Carter et al., "Radio Frequency Plasma Applications for Space Propulsion," *Int. Conf. on Electromagnetics in Advanced Applications*, 1999

[10] E. B. Hooper, "Plasma Detachment from a Magnetic Nozzle," *Journal of Propulsion and Power*, vol. 9(5), Sep. 1993

[11] N. Brenning, T. Hurtig, and M. A. Raadu, "Conditions for plasmoid penetration across abrupt magnetic barriers," *Phys. Plasmas*, vol. 12, no. 1, pp. 012309-1 – 012309-10, 2005

[12] C. K. Chu., "Magnetohydrodynamic Nozzle Flow with Three Transitions," *Physics of Fluids*, vol. 5(5), May. 1962., doi: 10.1063/1.1706656.

[13] S. A. Andersen et al., "Continuous Supersonic Plasma Wind Tunnel," *Physics of Fluids*, vol. 12, 1969., doi: 10.1063/1.1692519

[14] D. R. Otis., "Computation and Measurement of Hall Potentials and Flow-field Perturbations in Magnetogasydynamic Flow of an Axisymmetric Free Jet," *Journal of Fluid Mechanics*, vol. 24(1), pp.41-63, Feb. 1965., doi: 10.1017/S0022112066000508

[15] K. Kuriki and O. Okada., "Experimental Study of a Plasma Flow in a Magnetic Nozzle," *Physics of Fluids*, vol 13(9), pp.2262-2269, Sep. 1970., doi: 10.1063/1.1693232

[16] N. Gohda., "Interaction between a Shock-Heated Plasma and a Nozzle-Shaped Magnetic Field," *Journal of the Physical Society of Japan*, vol 46(4), Apr. 1979

[17] T. Kammash and M. Lee., "High-Thrust-High-Specific Impulse Gasdynamic Fusion Propulsion System," *Journal of Propulsion and Power*, vol. 13(3), May. 1997.

[18] R. P. Hoyt et al., "Magnetic Nozzle Design for Coaxial Plasma Accelerators," *IEEE Transactions on Plasma Science*, vol. 23(3), Jun. 1995.

[19] Y. D. Zhugzhada and V. M. Nakariakov., "Latent Heating of Coronal Loops," *Solar Physics*, vol. 175(1), pp.107-121, Sep. 1997

[20] K. F. Schoenberg et al., "Magnetohydrodyanmic Flow Physics of Magnetically Nozzled Plasma Accelerators with Applications to Advanced Manufacturing," *Physics of Plasmas*, vol. 5(5), May. 1998, doi: 10.1063/1.872880

[21] D.C. Black et al., "Two-dimensional Magnetic Field Evolution Measurements and Plasma Flow Speed Estimates from the Coaxial Thruster Experiment," *Physics of Plasmas*, vol. 1, May. 1994, doi: 10.1063/1.870503

[22] D.C. Black, R. M. Mayo, and R. W. Caress., "Direct Magnetic Field Measurement of Flow Dynamics in a Magnetize Coaxial Accelerator Channels," *Physics of Plasmas*, vol. 4, May. 1997, doi: 10.1063/1.872415

[23] N.F. Roderick et al., "Hydro magnetic Rayleigh-Taylor instability in high-velocity gas-puff implosions," *Physics of Plasma*, vol.5 (5), May. 1998

[24] H. Nakashima et al., "Use of an Ignition Facility for Fusion Propulsion Experiments," *Fusion Engineering and Design*, vol. 44, 1999

[25] R. A. Gerwin, "Integrity of the Plasma Magnetic Nozzle," *2010 Abstracts IEEE International Conference on Plasma Science*, 2010, doi:10.1109/PLASMA.2010.5534049

[26] A.V. Arefiev, and B.N. Breizman., "Collisionless Plasma Expansion into Vacuum: Two New Twists on an Old Problem," *Physics of Plasmas*, vol. 16, Apr. 2009, doi: 10.1063/1.3118625

[27] A.V. Arefiev and B.N. Breizman, "Ambipolar Acceleration of Ions in a Magnetic Nozzle," *Physics of Plasma*, vol. 15, Apr. 2008, doi: 10.1063/1.2907786

[28] A.V. Arefiev and B.N. Breizman, "Theoretical Components of the VASIMR Plasma Propulsion Concept," *Physics of Plasma*, vol. 11(5) May. 2004

[29] A. V. Arefiev and B. N. Breizman., "Magnetohydrodynamic Scenario of Plasma Detachment in a Magnetic Nozzle," *Physics of Plasmas*, vol. 12, Mar. 2005, doi: 10.1064/1.1875632

[30] P. G. Mikelides, P. J. Turchi, and N. F. Roderick., "Applied-Field Magnetoplasmadynamic Thrusters, Part1: Numerical Simulations Using the MACH2 Code," *Journal of Propulsion and Power*, vol. 16(5), Sep. 2000

[31] I.G. Mikellides et al., "Design of a Fusion Propulsion System-Part 2: Numerical Simulation of Magnetic Nozzle Flows," *Journal of Propulsion and Power*, vol. 18(1), pp.152-158, Jan-Feb. 2002

[32] M.Inutake et al., "Transonic Plasma Flow Passing Through a Magnetic Mirror," *Transaction of Fusion Science and Technology*, vol. 51, Feb. 2007

[33] M.Inutake et al., "Magnetic-Laval-Nozzle Effect on a Magneto-Plasma-Dynamic Arcjet," *American Institute of Physics*, Conference Proceeding 669, 2003

[34] M.Inutake et al., "Production of a High-Mach-Number Plasma Flow for an Advanced Plasma Space Thruster," *Plasma Science and Technology*, vol. 6(6), Dec. 2004

[35] M.Inutake et al., "Improvements of Flow Characteristics for an Advanced Plasma Thruster," *Transactions of Fusion Science and Technology*, vol. 27, Jan. 2005

[36] Y. Kajimura, R. Kawabuchi, and H. Nakashima, "Control Techniques of Thrust Vector for Magnetic Nozzle in Laser Fusin Rocket," *Fusion Engineering and Design*, vol. 81, 2006

[37] Y. Kajimura et al., "Numerical Simulation of Fusion Plasma Behavior in a Magnetic Nozzle for Laser Fusion Rocket," *Transactions of Fusion Science and Technology*, vol. 51, Feb. 2007

[38] Y. Kajimura et al., "Numerical Simulation of Plasma Behavior in a Magnetic Nozzle of a Laser-plasma Driven Nuclear Electric Propulsion System," *American Institute of Physics*, Conference Proceeding 1084, 2009

[39] J. Gilland et al., "Multi-Megawatt MPD Plasma Source Operation and Modeling for Fusing Propulsion Simulations," *American Institute of Physics*, Conference Proceeding 699, 2004

[40] J. Gilland, P. Mikellides, and D. Marriott, "Energy Deposition via Magnetoplasma-

dynamic Acceleration: I. Experiment," *Plasma Sources Science Technology,* vol. 18, 2009, doi: 10.1088/0963-0252/18/1/015001

[41] H. Tobari et al., "Characteristics of Electromagnetically Accelerated Plasma Flow in an Externally Applied Magnetic Field," *Physics of Plasmas*, vol. 14, Sep. 2007, doi: 10.1063/1.2773701

[42] G.S. Choi et al., "Development of Two Propulsion Systems with Helicon Plasma," *Transaction of Fusion Science and Technology*, vol. 51, Feb. 2007

[43] J. J. Brainerd and A. Reisz., "Electrodeless Experimental Thruster," *American Institute of Physics*, Conference Proceeding 1103, 2009

[44] R. Winglee et al., "Simulation and Laboratory Validation of Magnetic Nozzle Effects for the High Power Helicon Thruster," *Physics of Plasmas*, vol. 14, Jun. 2007, doi: 10.1063/1.2734184

[45] D.G. Chavers et al., "Momentum and Heat Flux Measurements Using an Impact Target in Flowing Plasma," *Journal of Propulsion and Power*, vol. 22(3) May-Jun. 2006

[46] A. Ando et al., "ICRF Heating and Plasma Acceleration with an Open Magnetic Field for the Advanced Space Thruster," *Transactions of Fusion Science and Technology*, vol. 51, Feb. 2007

[47] G. Vecchi et al., "A Simulation Approach for ICRF Plasma Thruster Antennas," *American Institute of Physics*, Conference Proceeding 787, 2005

[48] P.F. Schmit and N.J. Fisch, "Magnetic Detachment and Plume Control in Escaping Magnetized Plasma," *Journal of Plasma Physics*, vol. 75(3), pp. 359-371, Nov. 2008, doi: 10.1017/S0022377808007666

[49] F. N. Gest et al., "Ion Detachment in the Helicon Double-Layer Thruster Exhaust Beam," *Journal of Propulsion and Power*, vol. 22 (1) Feb. 2006

[50] R. Kawabuchi et al., "Numerical Simulation of Plasma Detachment from a Magnetic Nozzle by using Fully Particle-In-Cell Code," *Journal of Physics*, Conference Series 112, 2008, doi: 10.1088/1742-6596/112/4/042082

[51] B.N. Breizman, M.R. Tushentsov, and A.V. Arefiev, "Magnetic Nozzle and Plasma Detachment Model for a Steady-state Flow," *Physics of Plasmas*, vol. 15, Apr. 2008, doi: 10.1063/1.2903844

[52] M.D. West, C. Charles, and R.W. Boswell, "Testing a Helicon Double Layer Thruster Immersed in a Space-Simulation Chamber," *Journal of Propulsion and Power*, vol. 24 (1), Jan-Feb. 2008, doi: 10.2514/1.31414

[53] C.A. Deline et al., "Plume Detachment from a Magnetic Nozzle," *Physics of Plasmas*, vol. 16, Mar. 2009, doi: 10.1063/1.3080206

[54] T. Andreussi and F. Pegoraro., "Magnetized Plasma Flows and Magnetoplasmadynamic Thrusters," *Physics of Plasmas*, vol. 17, Jun. 2010, doi:10.1063/1.3447876

[55] E. Ahedo and J. Navarro-Cavalle., "Helicon Thruster Plasma Modeling: Two-dimensional Fluid-dynamics and Propulsive Performances," *Physics of Plasmas*, vol. 20, Apr. 2013, doi: 10.1063/1.4798409

[56] E. Ahedo and M. Merino., "Two-dimensional Supersonic Plasma Acceleration in a Magnetic Nozzle," *Physics of Plasmas*, vol. 17, Jul. 2010, doi: 10.1063/1.3442736

[57] E. Ahedo and M. Merino., "On Plasma Detachment in Propulsive Magnetic Nozzle," *Physics of Plasmas*, vol. 18, May. 2011, doi: 10.1063/1.3589268

[58] E. Ahedo and M. Merino., "Two-dimensional Plasma Expansion in a Magnetic Nozzle: Separation due to Electron Inertia," *Physics of Plasmas*, vol. 19, Aug. 2012, doi: 10.1063/1.4739791

[59] K. Takahashi, C. Charles, and R. W. Boswell., "Approaching the Theoretical Limits of Diamagnetic-Induced Momentum in a Rapidly Diverging Magnetic Nozzle," *Physical Review Letters 110*, May. 2013, doi: 10.1103/PhysRevLett.110.195003

[60] K. Takahashi, A. Komuro, and A. Ando., "Effect of Source Diameter on Helicon Plasma Thruster Performance and its High Power Operation," *Plasma Sources Science and Technology*, vol. 24, Aug. 2015, doi: 10.1088/0963-0252/24/5/055004

[61] K. Takahashi, A. Komuro, and A. Ando., "Low-pressure, High-density, and Supersonic Plasma Flow Generated by a Helicon Magnetoplasmadynamic Thruster," *Applied Physics Letters 105*, Nov. 2014, doi: 10.1063/1.4901744

[62] K. Takahashi, A. Chiba, and A. Ando., "Modifications of Wave and Plasma Structures by a Mechanical Aperture in a Helicon Plasma Thruster," *Plasma Sources Science and Technology*, vol. 23, Dec. 2014, doi: 10.1088/0963-0252/23/6/064005

[63] H. Lorzel and P. G. Mikellides., "Three-Dimensional Modeling of Magnetic Nozzle Processes," *AIAA Journal*, vol. 48(7), Jul. 2010, doi: 10.2514/1.J050123

[64] M.Merino and E. Ahedo., "Two-dimensional Quasi-double-layers in Two-electron-temperature, Current-free Plasmas," *Physics of Plasmas*, vol. 20, Feb. 2013, doi: 10.1063/1.4789900

[65] M.Merino and E. Ahedo., "Simulation of Plasma Flows in Divergent Magnetic Nozzles," *IEEE Transactions on Plasma Science*, vol. 39(11), Nov. 2011

[66] M. Merino. and E. Ahedo., "Plasma Detachment in a Propulsive Magnetic Nozzle via Ion Demagnetization," *Plasma Sources Science and Technology.*, vol. 23, May. 2014., doi: 10.1088/0963-0252/23/3/032001

[67] Y. Su, and K. C. Shaing., "Current-free Double Layers in Helicon Sources," *Plasma Sources Science and Technology*, vol. 20, Aug. 2011, doi: 10.1088/0963-0252/20/5/055008

[68] H. Tang et al., "Study of Applied Magnetic Field Magnetoplasmadynamic Thrusters with Particle-in-cell Code with Monte Carlo Collision. I.Computation Methods and Physical Processes," *Physics of Plasmas*, vol. 19, Jul. 2012, doi: 10.1063/1.4737098

[69] H. Tang et al., "Study of Applied Magnetic Field Magnetoplasmadynamic Thrusters with Particle-in-cell and Monte Carlo Collision. II. Investigation of Acceleration Mechanisms," *Physics of Plasmas*, vol. 19, Jul. 2012, doi: 10.1063/1.4737104

[70] N. Singh, S. Rao, and P. Ranganath., "Waves Generated in the Plasma Plume of Helicon Magnetic Nozzle," *Physics of Plasmas*, vol. 20, Mar. 2013, doi: 10.1063/1.4795734

[71] E. A. Bering III et al., "Observations of Single-pass Ion Cyclotron Heating in a Transsonic Flowing Plasma," *Physics of Plasmas*, vol. 17, Apr. 2010, doi: 10.1063/1.3389205

[72] B. W. Longmier et al., "Ambipolar Ion Acceleration in an Expanding Magnetic Nozzle," *Plasma Sources Science and Technology*, vol. 20, Jan. 2011., doi: 10.1088/0963-0252/20/1/025007

[73] J. P. Sheehan et al., "Temperature Gradients due to Adiabatic Plasma Expansion in a Magnetic Nozzle," *Plasma Sources Science and Technology*, vol. 23, Jul 2014, doi: 10.1088/0963-0252/23/4/045014

[74] M.Wiebold, Y. Sung, and J. E. Scharer., "Ion Acceleration in a Helicon Source due to the Self-bias Effect," *Physics of Plasmas*, vol. 19, May. 2012, doi: 10.1063/1.4714605

[75] M.Wiebold, Y. Sung, and J. E. Scharer., "Experimental Observation of Ion Beams in the Madison Helicon eXperiment," *Physics of Plasmas*, vol. 18, Jun. 2011, doi: 10.1063/1.3596537

[76] A. B. Sefkow and S. A. Cohen., "Particle-in-cell Modeling of Magnetized Argon Plasma Flow Through Small Mechanical Apertures," *Physics of Plasmas*, vol. 16, May. 2009, doi: 10.1063/1.3119902

[77] R. J. Goldston and P. H. Rutherford, "Introduction to plasmas" in *Introduction to Plasma Physics*, New York, NY, USA: Taylor and Francis Group, 1955, pp.1-3

[78] R. J. Goldston and P. H. Rutherford, "Single-fluid magnetohydrodynamics" in *Introduction to Plasma Physics*, New York, NY, USA: Taylor and Francis Group, 1955, pp.115-128

[79] J. D. Jackson, "Magnetostatics, Faraday's Law, Quasi-Static Fields" in *Classical Electrodynamics*, Third Ed. California, CA, USA: John Wiley and Sons, Inc. 1925, pp.174-236